J Appl Electrochem (2007) 37:805–812
DOI 10.1007/s10800-007-9315-3

ORIGINAL PAPER

Deposition and characterization of nickel–niobium composite electrocoatings

Alain Robin · R. Q. Fratari

Received: 11 September 2006 / Revised: 18 February 2007 / Accepted: 19 February 2007 / Published online: 23 March 2007

Abstract Ni–Nb composite electrocoatings were obtained on carbon steel from Watts bath, containing suspended 20 μm size niobium powders. The effect of cathodic current density, electrolyte stirring rate and concentration of Nb particles in the bath on the deposit morphology and texture, volume fraction of co-deposited Nb particles and microhardness was investigated. The Ni–Nb composite layers presented a rough morphology with randomly oriented Ni grains, whereas pure Ni coatings obtained under the same experimental conditions were smooth and showed highly preferred orientation in the [110] or [100] direction. Stirring rate of the electrolyte and concentration of Nb particles in the bath are the main parameters affecting the incorporation of Nb particles. The Nb incorporated volume fraction was 11–14%, 17–19%, 27–32% and 34–37% for the 20 g L^{-1} Nb/550 rpm, 20 g L^{-1} Nb/400 rpm, 40 g L^{-1} Nb/400 rpm and 40 g L^{-1} Nb/550 rpm conditions, respectively. The microhardness of the Ni–Nb composite coatings obtained at 20 and 40 mA cm^{-2} was higher than that of pure Ni layers, due to grain refining. Incorporation of Nb particles in Ni coatings improved the corrosion resistance of the deposits in NaCl and H_2SO_4 solutions.

Keywords Electroplating · Nickel · Niobium · Composite · Characterization

A. Robin (✉) · R. Q. Fratari
Departamento de Engenharia de Materiais/DEMAR, Escola de Engenharia de Lorena – Universidade de São Paulo/EEL-USP, Polo Urbo-Industrial, Gleba AI-6, 12600-000 Lorena, SP, Brazil
e-mail: alain@demar.faenquil.br

1 Introduction

Ceramics (SiC [1–6], Al_2O_3 [7, 8], TiO_2 [7, 9], ZrO_2 [7]), polymers (polyethylene [10], polytetrafluorethylene [11]), metals (Ti [12, 13], Al [14]) and other materials (hydroxyapatite [15], diamond [16]) have been co-electrodeposited with nickel in order to improve properties, such as hardness, wear resistance, lubrication, corrosion resistance and catalytic properties. The co-deposition consists in electrolyzing a nickel plating bath containing suspended solid particles using a suitable cathode material. The main parameters that influence the properties of the composites are electrolyte composition, pH, temperature, cathodic current density, stirring rate of the solution and particle concentration and size [17].

Electrodeposited Ni coatings are widely used for corrosion protection but present some limitations in acid solutions. Nb is more corrosion-resistant than Ni in almost all aqueous media [18]. Thus, it can be expected that the incorporation of Nb particles in a Ni matrix improves the corrosion resistance of the coatings.

The present work aims at the codeposition of electrolytic Ni and Nb powders by galvanostatic electrolysis in a Watts bath. The effect of cathodic current density, stirring rate and Nb particle concentration on Nb incorporation rate, deposit morphology and texture, and microhardness was studied. The corrosion resistance of the Ni–Nb composites in NaCl and H_2SO_4 solutions was also evaluated. The results were compared with those of pure Ni electrocoatings.

2 Experimental procedure

The Ni–Nb composites were prepared by constant current electrodeposition from a typical sulphate bath (Watts bath)

[19], containing 20 and 40 g L^{-1} Nb powders. The Nb powders were produced in-house by hydrogenation/dehydrogenation process [20] and their size ranged from 1 to 100 μm with a mean diameter of 20 μm. Figure 1 shows the morphology of the Nb particles. The specific area of the Nb powders was 0.4566 m^2 g^{-1} and their typical chemical composition was 30 wt-ppm Al, 100 wt-ppm Fe, 50 wt-ppm Si, 600–2,000 wt-ppm Ta, 6,000 wt-ppm O and 2,250 wt-ppm N. The microhardness of the Nb particles was 230± 15 VHN.

The bath composition and deposition conditions are listed in Table 1. Sheets of AISI 1020 carbon steel with 100 mm × 6 mm × 1 mm dimensions were used as cathodes. These were previously ground to a 600 grit finish, degreased and dried. Two electrolytic grade nickel sheets (100 mm × 20 mm × 5 mm) were used as anodes. The distance between the cathode and both anodes was about 25 mm. The bath was stirred by a magnetic stirrer with an agitation rate of 400 and 550 rpm and its temperature was maintained at 60± 2°C.

The plating times were 6 h 52 min, 3 h 26 min and 1 h 43 min for 10, 20 and 40 mA cm^{-2} cathodic current densities, respectively in order to produce coatings of approximately 100 μm thickness.

Scanning electron microscopy (SEM) (LEO VP-1450) was used to examine the surface morphology and the distribution of Nb particles in the deposits and X-ray diffractometry (XRD) (Siefert-Debyeflex 1001, Cu-Kα) was employed for compositional and texture analysis of the coatings.

The percentage of embedded particles in the deposits was determined from cross-sections photomicrographs using the free Scion Image Beta 4.02 software. The image analysis operations were performed at 500 times magnification on at least ten fields of view for each coating and the mean volume fraction of Nb was calculated.

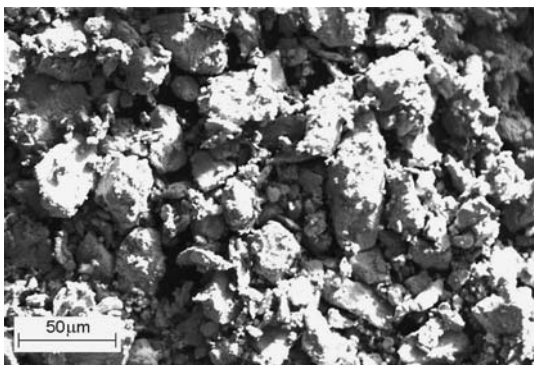

Fig. 1 SEM photograph of the Nb particles

Table 1 Bath composition and deposition conditions for Ni–Nb composite coatings

Bath composition	
Nickel sulphate ($NiSO_4$)	300 g L^{-1}
Nickel chloride ($NiCl_2$)	45 g L^{-1}
Boric acid (H_3BO_3)	40 g L^{-1}
Nb powder (20 μm size)	20 and 40 g L^{-1}
Deposition conditions	
Temperature	60± 2°C
pH	3.5
Stirring rate	400 and 550 rpm
Cathodic current density	10, 20 and 40 mA cm^{-2}

The roughness of the composite coatings was determined using a surface roughness measuring instrument (Mitutoyo SJ 201).

The microindentation hardness of the composite coatings was measured on polished cross-sections using a Vickers microhardness tester (Micromet 2004). A 100 g load was applied for 30 s.

The electrochemical behavior of pure Ni and Ni–Nb composite coatings was studied in naturally aerated and unstirred 3 wt.% NaCl (pH 6) and 20 wt.% H_2SO_4 solutions, using a typical three-electrode corrosion cell. The counter electrode was a square-shaped platinum sheet of 18 cm^2 area and the reference electrode was a saturated calomel electrode (SCE). Prior to polarization, the open-circuit potential was monitored until it reached steady state. Polarization measurements, performed using a PAR 273A potentiostat controlled with a microcomputer through M352 Corrosion Software, were carried out potentiodynamically at 1 mV s^{-1} potential sweep rate. The corrosion resistance of the coatings was evaluated from the corrosion current densities deduced from the polarization curves.

3 Results and discussion

3.1 Coatings morphology, texture and Nb particles content

Figure 2 shows the typical superficial morphology of Ni and Ni–Nb electrocoatings obtained for the same current density and stirring rate. As distinct from the smooth Ni coatings (Fig. 2a) which present a mean roughness of 1 μm, the Ni–Nb composite layers (Fig. 2b, c) have a rough morphology, constituted of nodular agglomerates. Larger agglomerates and rougher surfaces were obtained for the coatings obtained in 40 g L^{-1} Nb containing bath, whereas for both 20 and 40 g L^{-1} Nb the roughness tended to increase with increasing cathodic current density (Fig. 3). The rougher and nodular morphology of the

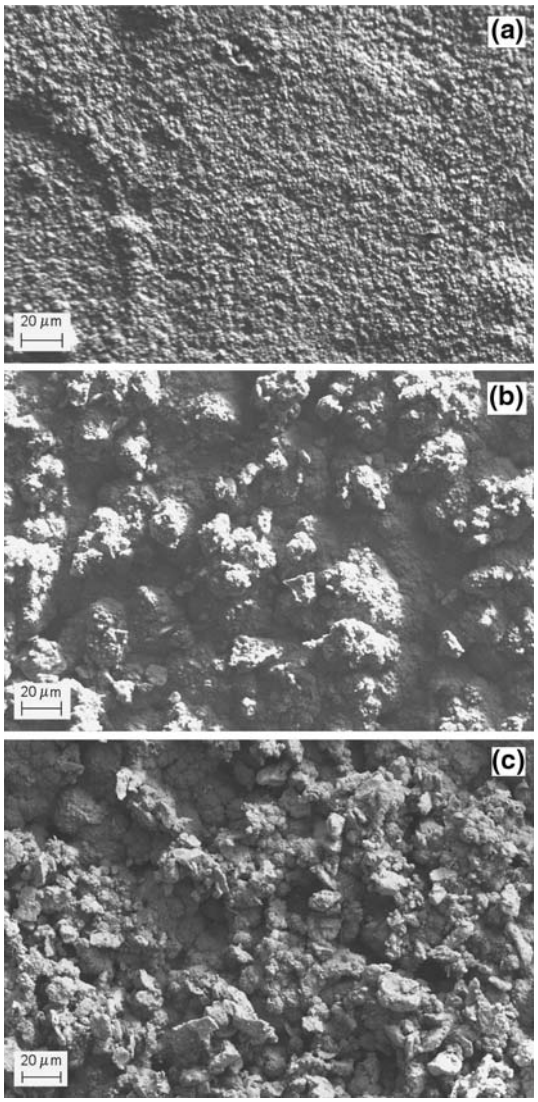

Fig. 2 SEM photographs of the surface of (**a**) pure Ni and (**b**, **c**) Ni–Nb composite coatings obtained using 10 mA cm^{-2} cathodic current density and 400 rpm stirring rate; (**b**) 20 g L^{-1} Nb concentration and (**c**) 40 g L^{-1} Nb concentration

composite layers when compared to pure Ni has been observed by others authors [3, 12, 13, 15, 16, 21]. This characteristic may be related to both the large size of the Nb particles used and the significant nucleation rate of new crystals on the particle surface before it is covered by the growing surrounding Ni layer.

From the SEM images using secondary electron mode (Fig. 4a), the deposited Ni and the Nb incorporated particles cannot be distinguished. Figure 4b shows a SEM image of the same region using a mixed secondary (20%)/backscattering (80%) electron mode with low image contrast. This allows differentiation of the chemical composition of the surface by atomic weight. In Fig. 4b, the white region corresponds to Nb (higher atomic weight) and

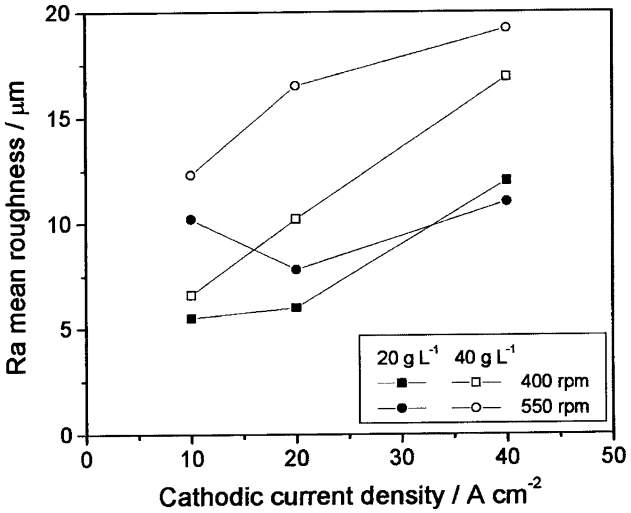

Fig. 3 Ra mean roughness of Ni–Nb composite coatings as a function of cathodic current density, stirring rate and Nb particle concentration

the black region to the Ni matrix (lower atomic weight). There is a good distribution of Nb on the coating surface, but only a few individual Nb particles can be distinguished, as most of the particles are partially or completely covered by metallic Ni.

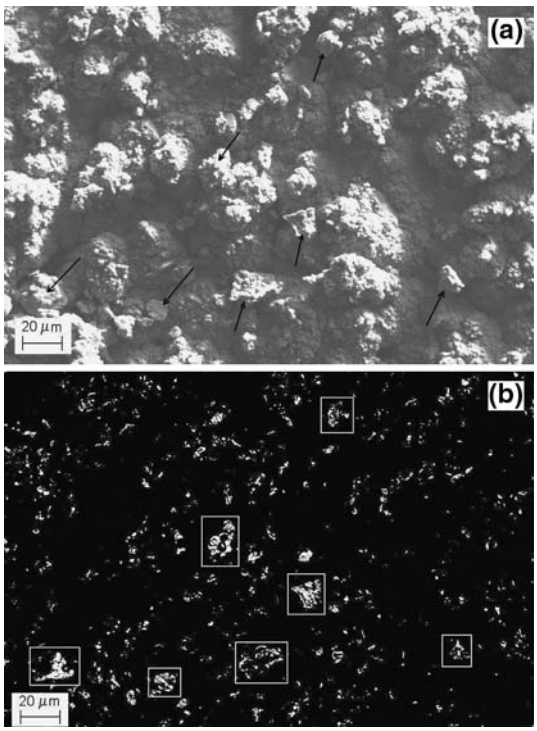

Fig. 4 SEM photographs of the surface of a Ni–Nb composite coating obtained at 10 mA cm^{-2} cathodic current density and 400 rpm stirring rate: (**a**) secondary electron mode and (**b**) mixed secondary (20%)/backscattering (80%) electron mode

Figure 5 shows the XRD patterns of Ni and Ni–Nb electrocoatings obtained for the same current density and stirring rate. As expected, the spectrum of the pure Ni layer only shows the diffraction peaks relative to the Ni phase, whereas the spectra of the composites reveal the presence of two phases, a Nb phase and a Ni phase from Nb embedded particles and Ni matrix, respectively. The higher intensity of the peaks relative to Nb for the deposit obtained in 40 g L^{-1} Nb containing bath (Fig. 5c) suggests a higher incorporation of Nb particles. Very similar XRD patterns were obtained for the composite coatings performed under other experimental conditions.

The orientation index was estimated using the following relation:

$$\text{Orientation index} = \frac{I_{hkl}/\sum I_{hkl}}{I_{ASTM\ hkl}/\sum I_{ASTM\ hkl}}$$

where I_{hkl} and $I_{ASTM\ hkl}$ are the integrated intensities from a (hkl) peak relative to Ni phase, obtained for the deposits and for nickel of random texture [22], respectively.

Figure 6 shows the orientation index of the (111), (200), (220) and (311) planes for pure Ni and Ni–Nb composite coatings (obtained in 20 g L^{-1} Nb containing solutions and 400 rpm stirring rate) as a function of cathodic current density. The Ni deposits are clearly textured in the [110] direction for both 10 and 20 mA cm^{-2} current density and in the [100] direction for 40 mA cm^{-2}. This observation is in accordance with published data [23], as the Ni coatings produced in Watts bath were shown to present the following order of texture, (110), (100) and eventually (210), when the deposition rate increases. When Nb particles are co-deposited the Ni grains do not now show preferential orientation, but rather a random orientation (Fig. 6). The present results agree with those of Stroumbouli [24] who recently showed that pure Ni deposit obtained in Watts bath for 70 mA cm^{-2} current density presented a high quality (100) preferred orientation, whereas Ni–WC composites obtained in the same conditions had an almost random orientation of Ni crystallites. The orientation of Ni grains in the Ni–Nb composites does not depend on cathodic current density, on stirring rate or Nb concentration, as similar orientation index values were calculated for the Ni–Nb coatings obtained in 20 g L^{-1} containing solutions at 550 rpm and in 40 g L^{-1} Nb containing solutions at both 400 and 550 rpm. Thus, it seems that the incorporation of Nb particles has perturbed the growth of the Ni matrix, probably due to the nucleation of randomly oriented new Ni crystals on the embedded Nb particles.

Figure 7a and b shows the cross-sections of composite layers obtained for the same cathodic current density and stirring rate in 20 and 40 g L^{-1} Nb containing baths, respectively. A good distribution of the Nb particles in the coatings shown in Fig. 7, as well as in the composites obtained in other experimental conditions, was noted.

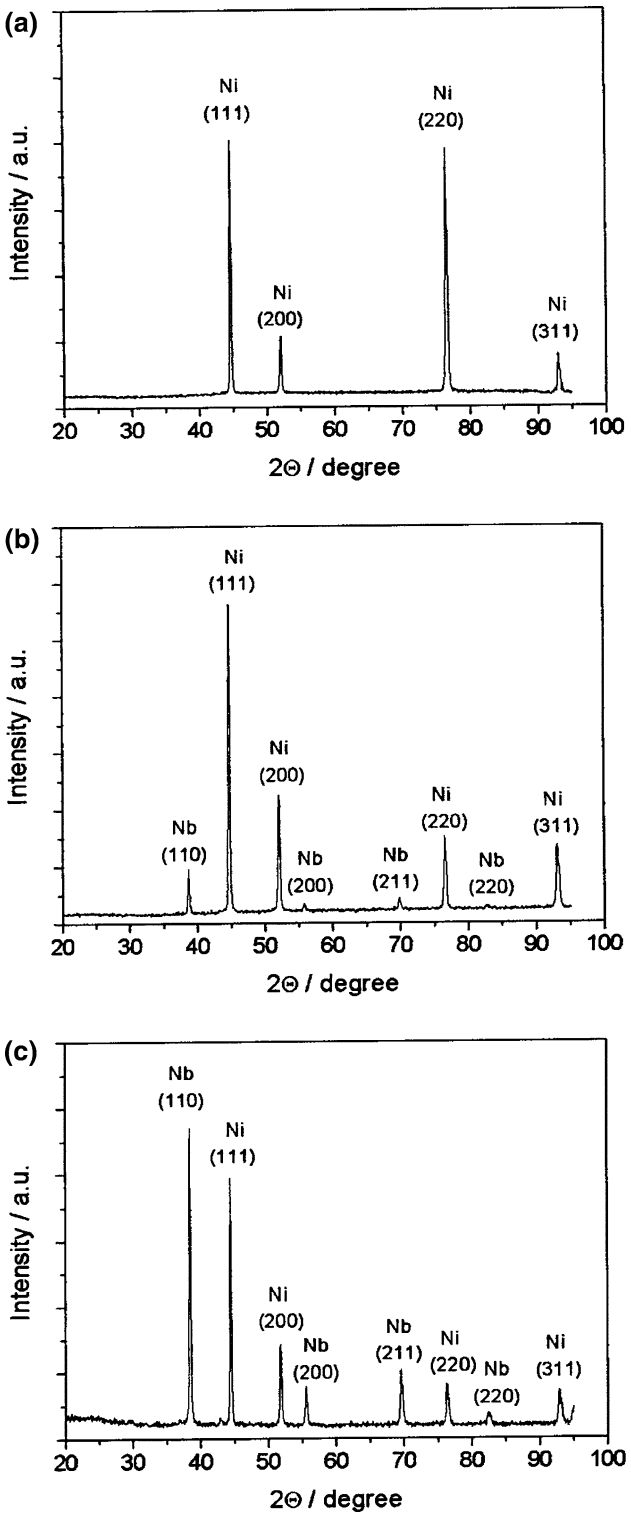

Fig. 5 XRD patterns of (**a**) pure Ni coating and (**b**, **c**) Ni–Nb composite coatings obtained using 10 mA cm^{-2} cathodic current density and 400 rpm stirring rate; (**b**) 20 g L^{-1} Nb concentration and (**c**) 40 g L^{-1} Nb concentration

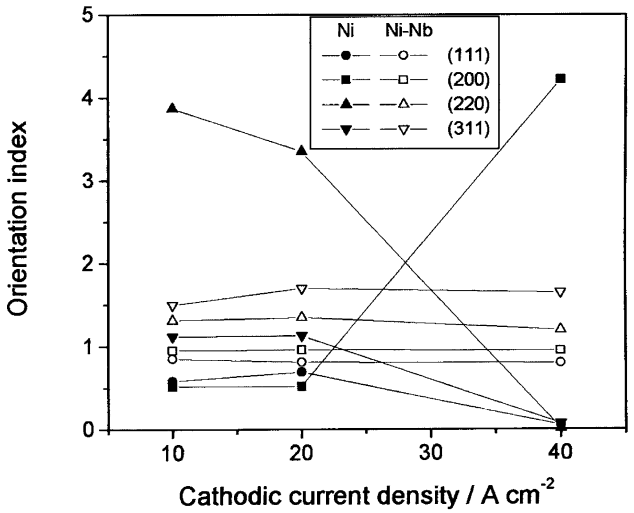

Fig. 6 Orientation index of Ni crystallographic planes for pure Ni and Ni–Nb composite coatings as a function of cathodic current density; Ni–Nb composites obtained in 20 g L^{-1} Nb containing solutions at 400 rpm stirring rate

Figure 7b depicts the higher incorporation of Nb particles for the composite obtained in 40 g L^{-1} Nb containing solution. The composite coatings were compact and no void at the steel/deposit interface, which could be harmful to adhesion, was observed. The good adhesion of the coatings was verified by bend test according to B 571-91 ASTM standard [25], as the Ni–Nb composite layers did not separate from the steel substrates, even after several bendings and breaking of the electroplated substrates.

The Nb incorporated volume fraction in the different composites, measured by image analysis, is presented in Fig. 8 as a function of cathodic current density, stirring rate and Nb particle concentration.

Higher Nb incorporation was measured for the composites obtained in 40 g L^{-1} Nb containing solutions. The increase in incorporated ceramic, polymeric or metallic particle fraction in Ni composite coatings with increasing particle concentration, with constant current density and stirring rate, has been shown by several authors [3, 6, 10–12]. As the hydrodynamic conditions used in this work were sufficient to maintain the Nb powders in suspension, higher particle concentration provided more collisions of particles against the cathode, resulting in an increase in Nb incorporation. Nevertheless, when the particles are not efficiently suspended under a given hydrodynamic condition, which is usual in solutions of very high particle content, an increase in particle concentration can decrease the particle incorporation [1, 9].

For a given stirring rate and Nb particle concentration, a slight decrease in incorporated Nb particle fraction occurred when the cathodic current density increased from 10 to 20 mA cm^{-2} (Fig. 8). This may be attributed to the

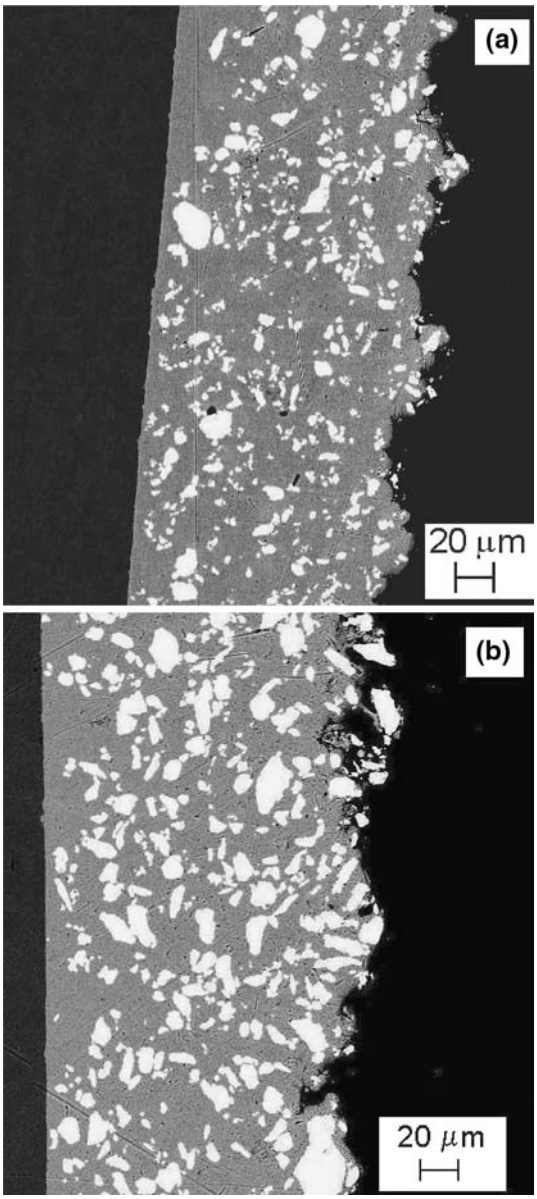

Fig. 7 SEM photographs of cross-sections of Ni–Nb composite coatings obtained using 40 mA cm^{-2} cathodic current density and 400 rpm stirring rate: (**a**) 20 g L^{-1} Nb concentration and (**b**) 40 g L^{-1} Nb concentration

increase in transport velocity of Ni ions to the cathode by diffusion (concentration overvoltage). As the velocity of Nb particle transport by mechanical agitation is maintained, this increase results in lower incorporated Nb fraction. Further increase in current density up to 40 mA cm^{-2} did not significantly affect the incorporation of Nb particles, which may mean that the Ni ion reduction rate was at its limiting value. Such effects of current density increasing on embedded particle fraction were also observed for the incorporation of SiC [1] and Al [14].

Several authors agree that there is an optimum stirring rate that leads to higher particle incorporation [1, 11, 26]. Up

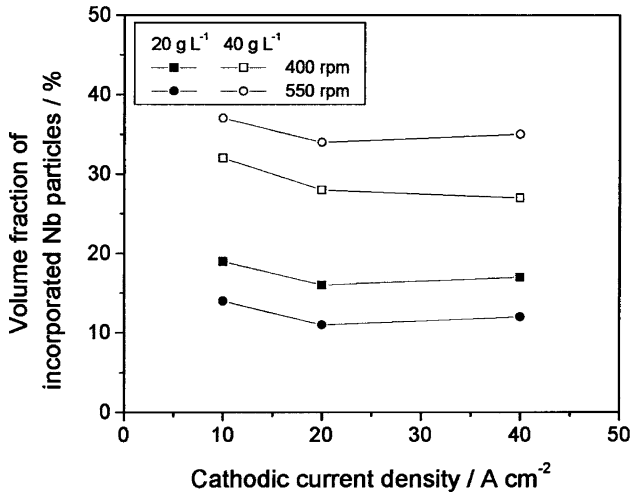

Fig. 8 Volume fraction of incorporated Nb particles as a function of cathodic current density, stirring rate and Nb particle concentration

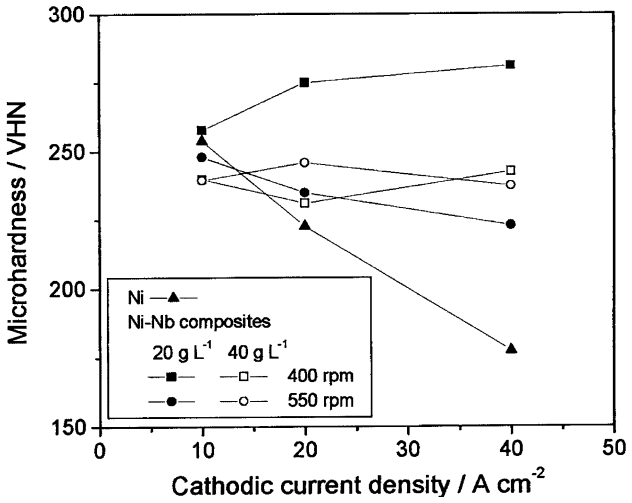

Fig. 9 Microhardness of Ni and Ni–Nb composite coatings as a function of cathodic current density, stirring rate and Nb particle concentration

to the optimum value, the collisions of particles against the cathode increase with increase in agitation rate, leading to an increase in the amount of co-deposited particles. Above the optimum value, the particles reaching the cathode surface may remove already adsorbed particles, resulting in a decrease in particle co-deposition. This optimum stirring rate was shown to increase with increasing particle concentration [11, 26]. In our investigated conditions, the higher Nb particle incorporation for 20 and 40 g L^{-1} Nb containing solutions was obtained at 400 and 550 rpm stirring rate, respectively, which is congruent with this trend.

From the data of Fig. 8, the stirring rate, as well as the Nb particle concentration have much more influence on the volume fraction of incorporated Nb particles than the cathodic current density.

3.2 Microhardness

Figure 9 shows the microhardness of the Ni–Nb composites as a function of cathodic current density, stirring rate and Nb particle concentration, as well as the microhardness of pure Ni layers for comparison. The microhardness of pure Ni decreases with increase in current density, as reported in the literature [27], and is associated with grain coarsening. The microhardness of Ni–Nb composites is close to the value measured for pure Ni when they were obtained using 10 mA cm^{-2} current density, but is higher when 20 or 40 mA cm^{-2} current densities were used. The difference between Ni–Nb composite and Ni hardnesses increases with increasing current density.

The higher microhardness of Ni-particles composites has been observed for almost all kinds of incorporated hard particles, such as SiC [2], Si_3N_4 [28], Al_2O_3 [29], and even for soft particles such as Al [14] and polyethylene [10]. There are three reasons for this increase in hardness: particle-strengthening [2, 28], dispersion-strengthening [2, 10, 29] and grain refining [10, 14]. Particle-strengthening is related to the incorporation of hard particles and volume fraction above 20%. In this case, the load is carried by both the matrix and the particles and strengthening is achieved because the particles restrain the matrix deformation. Dispersion-strengthening is associated with the incorporation of fine particles (<1 μm) and volume fraction lower than 15%. In this case, the matrix carries the load and the small particles hinder dislocation motion. The third mechanism is related to the nucleation of small grains on the surface of the incorporated particles, resulting in a general structural refinement. In this case, the presence of smaller grains impedes dislocation motion resulting in an increase in microhardness. The results cannot be explained by the first and second mechanisms, as an increase in microhardness was observed for particle volume fraction in the 11–17% range (composites obtained in 20 g L^{-1} Nb containing solutions), and the mean Nb particle size is much higher than 1 μm.

Figure 10 shows the microstructure of both pure Ni and Ni–Nb composite layers obtained at 40 mA cm^{-2} (and 20 g L^{-1} Nb concentration), after etching in a 5 mL HNO_3 + 2.5 mL CH_3COOH + 2.5 mL H_2O solution. The pure Ni coating has a characteristic columnar structure (Fig. 10a). A refining of the columnar grain structure in Ni deposits was observed as the current density decreased. Comparison of Fig. 10a and 10b clearly shows that the incorporation of Nb particles in a Ni matrix led to a change in microstructure from a columnar to a non-columnar structure and to general grain refining.

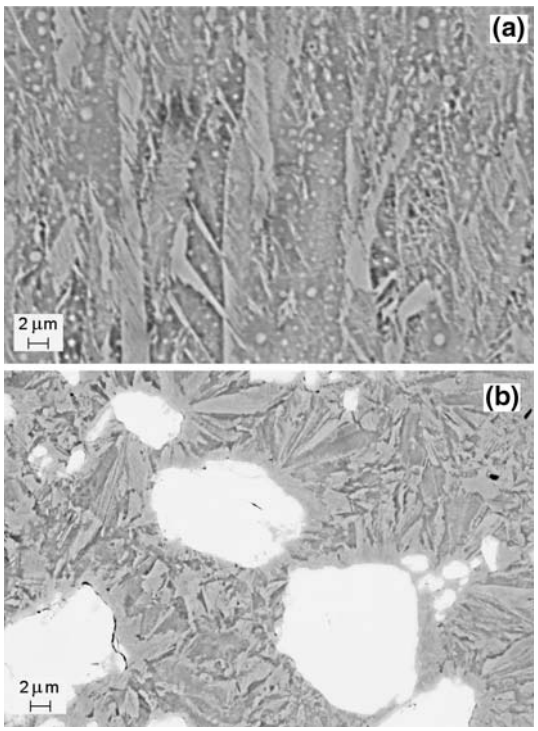

Fig. 10 SEM photographs of etched cross-sections of (**a**) pure Ni and (**b**) Ni–Nb composite coatings obtained using 40 mA cm^{-2} cathodic current density, 400 rpm stirring rate and for Ni–Nb composites, 20 g L^{-1} Nb concentration

This grain refining, which was observed for all the composites obtained using 20 and 40 mA cm^{-2} current density, may be due to the periodic nucleation of small Ni grains on the conductive surface of the Nb particles. The grain refining is less pronounced for the coatings obtained in 20 g L^{-1} containing solutions at 550 rpm, probably due to the lower incorporated Nb fraction. This results in a lower increase in microhardness for these composites. On the other hand, the microhardness of the composites obtained in 40 g L^{-1} Nb containing solutions, which have higher incorporated Nb fraction (27–35%), is lower than the microhardness of the composites obtained in 20 g L^{-1} Nb containing solutions at 400 rpm, that have an incorporated Nb fraction in the 16–17% range. For high Nb content deposits, the embedded particles begin to affect the microhardness more significantly than the Ni grain refining. This may explain why these composites have microhardness values (231–246 VHN) close to the hardness of the Nb particles (= 230± 15 VHN).

At the lowest current density (10 mA cm^{-2}), the grain size of pure Ni deposit is already small and cannot be significantly refined by Nb incorporation. Thus, very close microhardness values were measured for Ni and Ni–Nb composites obtained using 10 mA cm^{-2} (Fig. 9).

3.3 Corrosion resistance

Typical potentiodynamic polarization curves of pure Ni and Ni–Nb composite coatings of different incorporated particle volume fractions, obtained in 3% NaCl and 20% H_2SO_4 solutions at room temperature, are shown in Fig. 11a and 11b, respectively. Table 2 presents the values of the null-current potential $E_{i=0}$ and corrosion current density i_{corr}, the latter deduced by extrapolation of cathodic Tafel slopes. The Ni–Nb composites are more corrosion resistant than pure Ni layers and an increase in Nb particle volume fraction tends to decrease the corrosion current density in both salt and acidic media, thus improving the corrosion resistance. An increase in particle content for other composites obtained in Watts bath, such as Ni-polyethylene [10] and Ni-mica [30], was also shown to increase the corrosion resistance in NaCl solutions. On the other hand, Ni–SiC composites obtained from Watts bath [31] were more corrosion resistant than pure Ni in NaCl

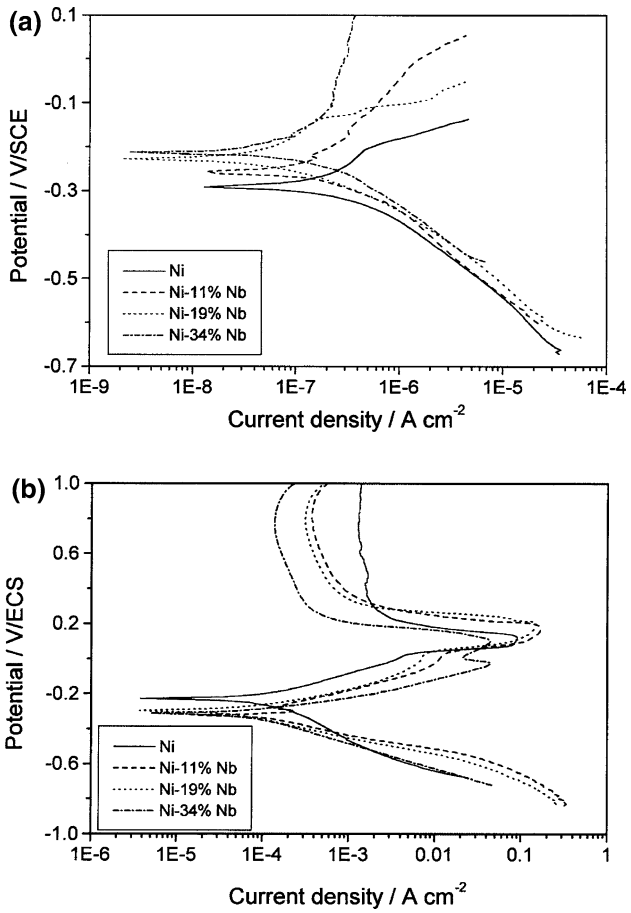

Fig. 11 Polarization curves obtained for pure Ni and Ni–Nb composite coatings of different Nb incorporated volume fraction in (**a**) 3 wt.% NaCl and (**b**) 20 wt.% H_2SO_4 solutions at room temperature

Table 2 Null-current potential $E_{i=0}$ and corrosion current density i_{corr} for pure Ni and Ni-11, 19 and 34% Nb composite coatings measured in 3% NaCl and 20% H_2SO_4 solutions at room temperature

Medium	Specimen	$E_{i=0}$ (V/SCE)	i_{corr} (μA cm^{-2})
3% NaCl	Ni	–0.291	0.5
	Ni-11%Nb	–0.257	0.3
	Ni-19%Nb	–0.228	0.2
	Ni-34%Nb	–0.213	0.2
20% H_2SO_4	Ni	–0.229	127
	Ni-11%Nb	–0.322	80
	Ni-19%Nb	–0.296	30
	Ni-34%Nb	–0.313	58

solutions, but their corrosion resistance was independent of the amount of incorporated particles.

The lower corrosion rate of Ni–Nb composites when compared to pure Ni may be attributed not only to the presence of Nb particles in the deposits, which intrinsically presents a higher corrosion resistance than Ni in most aqueous media, but also to the change in coating microstructure from columnar to non-columnar and small grain-size produced with particle incorporation. Such a change in microstructure, due to process conditions or to incorporation of solid particles, was shown to improve the corrosion resistance of the coatings [23, 31].

4 Conclusions

The Ni–Nb composite electrocoatings obtained from Watts bath containing suspended Nb powders presented a rough surface morphology with randomly oriented and small Ni grains. The pure Ni coatings obtained under the same experimental conditions were smooth, showed highly preferred orientation and presented a columnar structure.

Nb particle content in the bath and stirring rate had more influence on Nb incorporated volume fraction than cathodic current density.

The microhardness of the composite coatings was higher than that of pure Ni obtained under the same electrolysis conditions, due to grain refinement.

The corrosion resistance of Ni–Nb composites was higher than that of electrolytic Ni in NaCl and H_2SO_4 solutions.

Acknowledgements The authors are grateful to Prof. Dr. H.R.Z. Sandim (EEL-USP) for supplying the niobium powders and R.Q.F. acknowledges CNPq (Conselho Nacional de Desenvolvimento e Pesquisa – Brazil) for financial support.

References

1. Kim SK, Yoo HJ (1998) Surf Coat Technol 108–109:564
2. Garcia I, Fransaer J, Celis JP (2001) Surf Coat Technol 148:171
3. Medeliene V (2002) Surf Coat Technol 154:104
4. Zimmerman AF, Clark DG, Aust KT, Erb U (2002) Mater Lett 52:85
5. Hou KH, Ger MD, Wang LM, Ke ST (2002) Wear 253:1003
6. Socha RP, Laajalehto K, Nowak P (2002) Colloids Surf A 208:267
7. Wang SC, Wei WCJ (2003) Mater Chem Phys 78:574
8. Steinbach J, Ferkel H (2001) Script Mater 44:1813
9. Zhou M, Tacconi NR, Rajeshwar K (1997) J Electroanal Chem 421:111
10. Abdel Hamid Z, Ghayad IM (2002) Mater Lett 53:238
11. Berçot P, Peña-Muñoz E, Pagetti J (2002) Surf Coat Technol 157:282
12. Serek A, Budniok A (2002) Curr Appl Phys 2:193
13. Panek J, Serek A, Budniok A, Rówinski E, Lagiewka E (2003) Int J Hydrogen Energy 28:169
14. Susan DF, Barmak K, Marder AR (1997) Thin Solid Films 307:133
15. He L, Liu H, Chen D, Chen Z, Bai X (2002) Surf Coat Technol 160:109
16. Lee WH, Tang SC, Chung KC (1999) Surf Coat Technol 120–121:607
17. Hovestad A, Janssen LJJ (1995) J Appl Electrochem 25:519
18. ASM Handbook (1993) Corrosion, vol 13. ASM International, Materials Park
19. ASM Handbook (1994) Surface engineering, vol 5. ASM International, Materials Park
20. Sandim HRZ (1996) Preparation of Nb-TiO_2 alloys by powder metallurgy and its microstructural characterization. PhD Thesis, Universidade de São Paulo
21. Losiewicz B, Budniok A, Rówinski E, Lagiewka E, Lasia A (2004) J Appl Electrochem 34:507
22. Selected Powder Diffraction Data-Metals and Alloys-Data Book (1978) JCPDS International Centre for Diffraction Data, Swarthmore
23. Dini JW (1993) Electrodeposition: the materials science of coatings and substrates. Noyes Publications, Park Ridge
24. Stroumbouli M, Gyftou P, Pavlatou EA, Spyrellis N (2005) Surf Coat Technol 195:325
25. Annual Book of ASTM Standards (1992) Volume 02.05, ASTM International
26. Wang H, Yao S, Matsumara S (2004) J Mater Proc Technol 145:299
27. Safranek WH (1974) The properties of electrodeposited metals and alloys. Elsevier, New York
28. Ramesh CS, Seshadri SK (2003) Wear 255:893
29. Ferkel H, Müller B, Riehemann W (1997) Mater Sci Eng A 234–236:474
30. Rethinam AJ, Ramesh Bapu GNK, Krishnan RM (2004) Mater Chem Phys 85:251
31. Garcia I, Conde A, Langelaan G, Fransaer J, Celis JP (2003) Corr Sci 45:1173